Reduced-Order Thermal Behavioral Model Based on Diffusive Representation

Bruno Allard, *Senior Member, IEEE*, Xavier Jordà, Pierre Bidan, Axel Rumeau, Hervé Morel, *Senior Member, IEEE*, Xavier Perpiñà, Miquel Vellvehi, and Sabrine M'Rad

***Abstract*—The virtual prototyping of power electronic converters requires electrothermal models with various abstraction levels and easy identification. Numerous methods for the construction of compact thermal models have been presented in this paper. Few of them propose state-space models, where the model order can be controlled according to the necessity of the virtual prototyping analyses. Moreover, the model reduction methods require the experience of the engineer and previous calibration. Diffusive representation (DR) is proposed here as an original and efficient method to build compact thermal models as state-space models. The model reduction is obtained through the model parameter identification and/or the time horizon of the measurement data provided for the identification. Instead of eigenvalue elimination, the method enables to specify adequately inside the model the frequency domain wished for the virtual analysis at hand. The proposed method is particularly dedicated to the system optimization phases. Experimental and simulation results are in good agreement. The advantages and limitations of the DR are discussed in comparison to published methods.**

***Index Terms*—Diffusive representation (DR), electrothermal effects, reduced-order systems.**

I. Introduction

THIS PAPER addresses a modeling method to represent the electrothermal behavior of a power system with respect to virtual prototyping. A power system is considered to be an assembly of converters supplying energy to actuators irrespective of their final energy domains. A primary power supply offers the energy processed by the power electronic converters. Sensors feed controllers with necessary information. Many physical phenomena appear in such power systems, and integration only couples these phenomena in a tighter manner.

Integration of power systems is a technological response to the necessity of higher efficiency, but lower cost or concurrent mass production. As physical prototyping becomes less and less affordable with integration level, there is a growing interest in virtual prototyping. A simulation-driven product-development cycle defines the steps required to deliver a fully qualified product starting from the product specification sheet. The virtual prototyping is considered here as the ensemble of simulation tools and related procedures to deliver a pertinent product solution at the beginning of the first physical validation step of the development cycle. In an ideal case, the virtual prototype must guarantee the highest level of confidence in the product development results. A lot of analyses should be carried out through simulation and a wide variety of models are required. The challenges lay with the choice and ordering of analyses, and the modeling approaches including the model parameter identification.

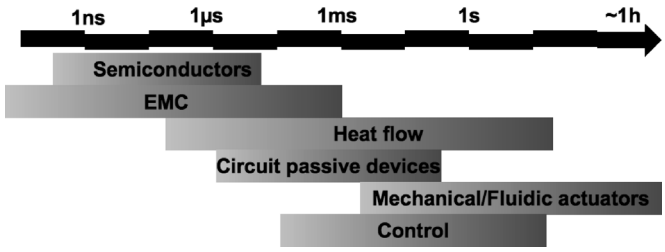

Fig. 1. Main blocks of a power system ordered with respect to the main time-constant values.

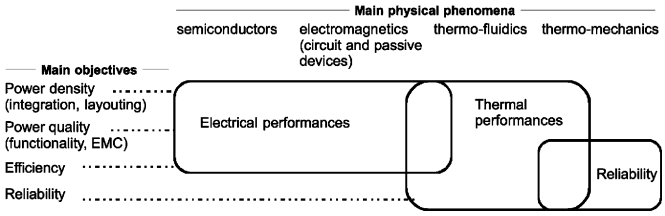

Fig. 2. Relations between some main physical phenomena and prototyping issues.

The physical phenomena inside a power system can be seen through their main time constants that appear to be broadly spreaded. Fig. 1 shows the main ranges of some time constants. Regarding the sole power electronic converter, Fig. 2 shows the physical phenomena that should be considered for some main analyses in virtual prototyping. The design objectives address the converter efficiency, power density (integration issue), power quality (functionality and interaction with outside system), and reliability. These objectives are evaluated with specific analyses and proper models should be selected. The models should encompass the required physical phenomena, and Fig. 1 indicates that the model formulations will be complicated as a wide range

Manuscript received March 7, 2009; revised May 20, 2009. Current version published December 28, 2009. Recommended for publication by Associate Editor B. Lehman.

B. Allard, H. Morel, and S. M'Rad are with Université de Lyon, Institut National des Sciences Appliquées – Lyon, Laboratoire Ampère, Centre National de la Recherche Scientifique, UMR 5005, F-69621 Villeurbanne, France (e-mail: bruno.allard@insa-lyon.fr).

X. Jordà, X. Perpiñà, and M. Vellvehi are with the Instituto de Microelectrónica de Barcelona, Centro Nacional de Microelectrónica (Spanish Council for Research), 08193 Barcelona, Spain.

P. Bidan and A. Rumeau are with the Laboratoire Plasma et Conversion de l'Energie Laboratory, Centre National de la Recherche Scientifique Unité Mixte de Recherche 5213, University of Paul Sabatier, 31062 Toulouse, France.

Color versions of one or more of the figures in this paper are available online at http://ieeexplore.ieee.org.

Digital Object Identifier 10.1109/TPEL.2009.2028231

of time constants appears. On one hand, the electrical performances and reliability analyses are quite decorrelated, and then can be evaluated one after the other. One the other hand, the thermal performances are correlated to some electrical performances of the system, namely, the power losses in a way and the impact of temperature in the other way. This concludes that the models necessary for the evaluation of the thermal performances of a power electronic converter are complex. Virtual prototyping performs through different abstractions or levels, and models should be adequate as well.

Numerical methods like finite-element modeling (FEM) are part of the most accurate approaches to couple electrical, thermal, and mechanical issues. However, the simulation cost limits the usage of FEM for predesign and optimization steps. A low-level abstraction is presented in [1], where a 3-D-FEM is considered, but the analyses are limited to the transient electrothermal behavior of the power converter. More compact models are then required. FEM is not discussed here, and the proposed method concerns efficient, behavioral, state-variable thermal modeling for heterogeneous electrothermal simulation.

Integration in power electronics makes the electrothermal modeling problem quite similar in complexity with the one in packaged ICs. Dynamic compact thermal models are to be seen first in the latter area and the development has a long history. For example, a review can be found in [2]. Concerning power semiconductor devices, the modeling approach intends to incorporate the impact of temperature, and junction temperatures are then generally considered. The electrothermal models evaluate power losses at specific locations of injection of heat into the thermal path system. The thermal model of the thermal path is the other important part of the electrothermal model.

The open issues in electrothermal modeling are the material parameters, the boundary conditions (BCs), the abstraction levels, and the accuracy/cost ratio or model reduction.

A. Material Parameters

The devices inside a power converter comprise various materials whose thermal behavior are nonlinear. However, it has been demonstrated in [3] that, considering linear material, parameter introduces only 3% error compared to nonlinear parameters if the temperature rise is less than 80 °C, which is the limitation introduced by silicon (the limiting material so far in a power converter). The material parameter linearity is an acceptable assumption.

B. Abstraction Levels and Boundary Conditions

In microelectronic domain, thermal approaches have first covered the modeling of standard package thermal behavior, where one internal junction temperature is considered [4], [5]. More recently, modeling has been extended to an unlimited number of hotspots for large IC module analysis [6], IC layouting objectives [7], or because of the heterogeneous nature of system in packages [8], [9].

In power electronics, approaches cover the thermal modeling for the simulation coupling of the electrical part and the thermal system part. Modeling differs only if a limited number of temperatures are to be monitored or if the temperature field is required. *Kojima et al.* [10] address the monitoring of the silicon device temperature inside the inverter of a hybrid vehicle with respect to a mission profile of the vehicle. This high-level abstraction is based on a static network representation of the thermal behavior of the power converter. The thermal impedance, Z_{th}, between the temperature to monitor and the device power losses are defined as multiexponential sums. The same approach is successfully applied in [11].

A Foster network is then identified through FEM intensive simulation of the material assembly of the power converter solicited by power pulse in the kilohertz range. BCs are included in the static network. The compact thermal model enables affordable simulations in the second-to-minute range of system operation with an acceptable accuracy. The generalized pencil of function presented in [12] is a similar approach though it is part of a broader procedure that includes a reduction step, as evocated later. Rencz coworkers [13], [14] introduce so-called structure functions to generate a Cauer network of heat flow paths. This offers a better understanding of the heat flow path behavior *a priori* as it is closer to physics, but it is less adequate for identification and model reduction. Thus, it does not bridge significant improvement with respect to previous approaches.

Development like [15] explores a way to build the heat flow path model from the system geometry. Each layer of the system is sliced into simple geometric forms to which correspond network equivalents. The final network is obtained by assembly of the various portions. The procedure detailed in [16] intends to bring the gap between 3-D-FEM and 1-D representation for the cosimulation of electrical and thermal models. The method offers quite advantages, but requires a lot of experience from the user. This is a limitation with respect to design optimization, where the thermal model needs to be rebuilt or identified at each step. A similar path between numerical modeling and a static network model is presented in [17] using a parametric model reduction method developed previously for transmission line modeling. The method appears efficient, but necessitates the access to the set of equations of the numerical model plus the user experience to guide the model reduction.

Some of the aforementioned works consider fixed and temperature-independent BCs. This assumption is acceptable only for a limited time duration and given system environment. A power converter is based on power modules and passive components attached to a mechanical substrate. Power losses are generated by the power semiconductor devices and the power devices. The heat flow path makes the silicon or the inner part of passive devices heat first, and then cool with time when the heat reflows inside the thermal assembly. Not all the thermal assembly is solicited at the same time. So, depending on the analysis time window, a specific thermal model is required. The thermal model BCs should then be time-dependent. In [18], BCs are represented by surface heat sources, arbitrary number of thermal contact, and nonuniform heat transfer coefficients, as detailed in [19]. The idea of listing exhaustively the possible BCs of a system has been explored [20], but does not offer a pertinent solution to the situation of an integrated power system where

BCs change fastly in types and values. Green function representation is also proposed in [18] instead of multiexponential sum representation. The temperature, anywhere in the system, can be extrapolated with sufficient accuracy. Authors use least-square fit of measured to simulate heating curves to identify the Green function parameters.

C. Model Reduction

Whatever the canonical form of the thermal model is, it is an important issue to reduce the model validity range in time and space according to the analysis problem at hand. Model reduction has received a lot of attention in literature: Padé approximant problems [21], Arnoldi approximant method [22], proper orthogonal decomposition [23], Fourier model reduction [24], bounded eigenvalues [25], parametric model reduction [17], or Krylov subspace method [26]. Whatever the method, the objective is to remove the maximum of terms or functions, but preserving an acceptable accuracy to the model, i.e. keeping the representation of the *modes* involved in the analysis at hand [27].

Recent proposed methods are based on Krylov subspace method. Basically, the method considers the pole/residue representation and the assumption of conjugate pairs to alleviate the stability requirement. A state-space representation is then realized and the reduction is performed. The reduced state-space representation is converted again in partial fraction form or, whatever, the initial representation. Gerstenmaier *et al.* [18] apply their method to a dc/dc converter where the thermal model order is initially of 20, and is arbitrarily reduced to 11 for convenience with PSPICE simulator convergence requirements. The multiexponential sums are increased in number to take care of parasitic conduction paths in [13]. The model reduction is no more possible, which enlightens the difficult task to dose the reduction effort with respect to the awaited accuracy of the thermal model. Removing the smallest eigenvalues in the thermal impedance, expression like (1) introduces errors in the temperature estimation at various locations. It is generally acceptable, but it shows that small and large eigenvalues are mixed, whatever is the time range of the system operation to simulate

$$Z(\vec{r},t)=\sum_{i=1}^{\infty}\Phi_i(\vec{r})\alpha_i\tau_i(1-e^{-t/\tau_i}) \tag{1}$$

where α_i represents the amplitude associated to the corresponding eigenvectors Φ_i and τ_i is a time constant. The hot spot temperature is evaluated using the following general relation

$$T(\vec{r},t)=\sum_{i=1}^{\infty}\delta_i(t)\Phi_i(\vec{r}). \tag{2}$$

The first main interest of the proposed method, so-called *diffusive representation (DR)*, is a clear insight into the model reduction, i.e., the model order. DR produces a state-space representation of the thermal model, and the identification of the model parameter is straightforward and addresses any desired abstraction of representation.

A logarithmic timescale is used in [12] and [18] instead of a linear sampling of the measurements from which are identified the thermal model parameters. At very small timescale, i.e., suitable for the analysis of semiconductor device electrothermal behavior, it appears that the thermal response does not go to nonzero immediately after the beginning of power losses generation ($t \geq 0$). With most published methods, the thermal model is identified with the same measurement data for small and large timescale. Using a linear sampling of data would mean large matrix size. A logarithmic timescale reduces the matrix size, but model reduction concerns a further restriction of the thermal model order with respect to the analysis-suitable timescale. The second main interest of the proposed method is that the manipulated matrices have the exact size required by the compact model: the model construction does not use a primary large size representation that is reduced afterward. The identification methods take care of the required timescale introduced by the electrothermal analysis at hand.

DR is an original mathematical framework suitable for any diffusion-based physical phenomena. It has been applied successfully to electromagnetic problems [28]–[31]. The application to thermal problem is detailed in three sections. Next section exposes the theoretical basis of DR and the development from a lumped representation to a discrete representation. The identification procedure is detailed. Section III introduces a specific test bench developed for the experimental validation of the proposed thermal model in the case of one power source and one temperature to monitor. Section IV covers the application of DR to the case of coupled thermal sources. The extrapolation to multisources/multihot spots is then straightforward. The method's advantages and limitations are compared to published procedures and discussed in Section V. The proposed method builds compact thermal model using a systematic procedure, and simulation results are in good agreement with experimental results in the frame of power converter design.

II. Diffusive Approximation Theoretical Issues

The concept of *DR* was introduced in [32] and extended to a general framework in [33] for the construction of dynamic realizations of causal nonrational operators. Nonrational operators correspond to infinite-dimension partial differential equations. The application presented in this paper can be seen as a suitable restriction of the general theory. Various details and extensions will be found in [33] and [34]. Applications may be found in [35].

A. General Formulation

Given a (nonrational) transfer function, $H(p)$, associated with a convolutive *causal* operator denoted by $H\left(\partial_t\right)$, the *canonical diffusive realization* of this operator is expressed, *when it exists*, by the following input (u)–output (y) (infinite dimensional) state realization of $u \mapsto y = H\left(\partial_t\right) u = h * u$:

$$\begin{cases} \dfrac{\partial\psi(t,\xi)}{\partial t} = -\xi\,\psi(t,\xi) + u(t),\ \psi(0,\xi)=0, & \xi>0 \\ y(t)=\displaystyle\int_0^{+\infty}\eta(\xi)\,\psi(t,\xi)\,d\xi \end{cases} \tag{3}$$

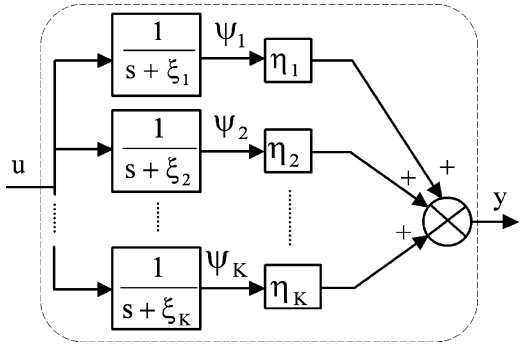

Fig. 3. Block diagram for Laplace transform of (7).

where $\eta(\xi)$, the so-called *diffusive symbol* of $H(\partial_t)$, is a solution of the following integral equation directly obtained from Laplace transform (with respect to t):

$$H(i\omega) = \int_0^{+\infty} \frac{\eta(\xi)}{i\omega + \xi}\, d\xi, \qquad \omega \in \mathbf{R}^*. \tag{4}$$

Function ψ is called the *DR* of u. It is, indeed, a (time frequency) representation of the input only.

Note that the complexity of (3) is intermediate between ordinary differential equations and partial differential ones. As a consequence, dynamic richness of partial differential operator (PDO) and straightforward rational approximations will be at the same time available under this unified form.

The impulse response $h := \mathcal{L}^{-1}H$ is clearly expressed from η

$$h(t) = \int_0^{+\infty} e^{-\xi t}\eta(\xi)\, d\xi = (\mathcal{L}\eta)(t) \tag{5}$$

so the diffusive symbol η is also given by [33]

$$\eta = \mathcal{L}^{-1}h. \tag{6}$$

Remark: The origin of the term "DR" is the diffusion equation or heat equation; see [34] for more details.

B. Finite-Dimensional Approximations

Finite-dimensional approximations of $H(\partial_t)$ can then be constructed using a discretized ξ-variable and applying a standard quadrature methods on (3) or (4). This leads to input–output approximations $u \mapsto \tilde{y} \simeq y = H\left(\frac{d}{dt}\right) u$ of the following form:

$$\begin{cases} \dfrac{d\psi_k(t)}{dt} = -\xi_k\, \psi_k(t) + u(t), \quad \psi_k(0) = 0, \quad k = 1, \ldots, K \\ \tilde{y}(t) = \displaystyle\sum_{k=1}^{K} \eta_k\, \psi_k(t) \end{cases} \tag{7}$$

whose similarity with (3) allows to deal with numerical approximation problems in a unified framework. The block diagram proposed in Fig. 3 is obtained by applying Laplace transform to system (7). It pictures the filtering effect of ξ-variable and weight effect of the diffusive symbol η.

In practice, small K (about 10–30) are sufficient to get satisfying approximations. This latter point is essential, namely, for long-memory operators whose standard approximations based on the convolutive expression generally lead to algorithms of great numerical complexity.

C. Identification of the Diffusive Symbol in Time Domain

1) Principle: The identification problem is to get the diffusive symbol $\eta(\xi)$ from experimental (time domain) data on the operator $H(\partial_t)$. Then from (3), we obtain a state-space realization of this operator. In practice, this problem is solved from physical measurements with limited precision, so that (4) must be replaced by a weakened problem, namely, an optimization one. Given a known input, $u(t)$, and a set of output measurements with error, v, we consider the mapping $\mathbf{A}$

$$\eta \mapsto \mathbf{A}(t)\,\eta(\xi) := \int_0^{+\infty} \eta(\xi)\, \psi(t, \xi)\, d\xi \tag{8}$$

where ψ is defined by the dynamic equation (3), and of the output measurement, $\mathbf{Y}$, is

$$\mathbf{Y} := y(t) + v(t). \tag{9}$$

The identification problem is to yield a solution, $\widehat{\eta}$, for the following equation (inverse problem):

$$\mathbf{Y} = \mathbf{A}\eta. \tag{10}$$

The solution of (10) by least-square approach is given by

$$\widehat{\eta} = (\mathbf{A}^\star\mathbf{A})^{-1}\mathbf{A}^\star\mathbf{Y}. \tag{11}$$

The estimated output

$$\widehat{\mathbf{Y}} = \mathbf{A}\widehat{\eta} \tag{12}$$

corresponds to the orthogonal projection of Y on A.

2) Finite-Dimensional Formulation: A finite-dimensional formulation must be used in order to tackle with experimental data. Numerical solutions impose a discretization of the ξ-axis, so that the identified diffusive symbol is searched as

$$\eta(\xi) = \sum_{k=1}^{K} \eta_k\, \delta(\xi - \xi_k) \tag{13}$$

where $\delta(x)$ denotes the Dirac distribution at point x. The mesh $\{\xi_k\}_{1\le k\le K}$ is chosen in accordance with the dynamic features of the system (i.e., the useful spectral contents of the experimental measurements): a geometric sequence is often well adapted. The frequency mesh is obviously limited by the identification measurement resolution on one hand, and the time response overall frequency bandwidth on the other hand.

From a finite number of data available on the temporal mesh $[t_m]_{1\le m\le M} \subset \mathbf{R}^+$ and using the earlier discretization (13) of the diffusive symbol, we denote

$$\begin{aligned} y_m &= y(t_m) \quad A_{m,k} = \psi_k(t_m) \\ &= \psi(t_m, \xi_k) = \int_0^{t_m} e^{-\xi_k(t_m - \tau)} u(\tau)\, d\tau. \end{aligned} \tag{14}$$

With vector $\eta := [\eta_k]_{1\le k\le K} \in \mathbf{R}^K$ and the matrix $\mathbf{A} := [A_{m,k}]$, the least-square problem is then transformed into the

finite dimensional one as

$$\min_{\eta\in\mathbf{R}^K}\sum_{m=1}^{M}|(\mathbf{A}\eta)_m - y_m|^2. \tag{15}$$

3) Case of Ill-Conditioned Matrix $\mathbf{A}^\star\mathbf{A}$*:* Under its ideal formulation, the identification problem is often excessively sensitive to numerical errors because the matrix $\mathbf{A}^*\mathbf{A}$ is closed to a noninversible one. This is namely the case when $\xi_1 \ll \xi_K$, i.e., when identification is significant on a frequency band covering several decades. As usual, the following reconditioned problem with small parameter $\varepsilon > 0$ can then be judiciously considered in place of the least-square problem

$$\min_{\eta}\{\|\mathbf{A}\eta - \mathbf{Y}\|^2 + \varepsilon\|\eta\|^2\} \tag{16}$$

the solution of which is classically given by ($\mathbf{I}$ denotes the identity matrix)

$$\widehat{\eta} = [\mathbf{A}^\star\mathbf{A} + \varepsilon\mathbf{I}]^{-1}\,\mathbf{A}^\star\mathbf{Y}. \tag{17}$$

The parameter ε is chosen as small as possible as long as $\widehat{\eta}$ remains quasi-insensitive to important relative variations of ε. In practice, very small ε are sufficient to stabilize the problem, and the estimated output $\widehat{\mathbf{Y}}$ [(12)] are both very close[1] to the ideal one and robust to numerical errors.

As a conclusion, the theoretical framework of DR may be applied to a practical engineering problem, providing a finite discretization formulation and a suitable identification of the model parameters. Next sections introduce the one-input/one-output problem, and then, the two-inputs/two-outputs problem what is sufficient to demonstrate the application of the method to a problem of any size.

III. One-Input/One-Output Model

DR is proposed here for the construction of compact thermal models of power converters made of power modules. Two main kinds of substrates are used in typical power converter assemblies. Direct copper-bonded (DCB) ceramic substrates are preferred for high power applications. Basically, they consist of a copper-ceramic layer-copper sandwich structure. Alumina and aluminum nitride ceramic layers show very good thermal properties, although their mechanical properties are not optimal and the AlN cost is relatively high. Insulated metal substrates (IMSs) represent an interesting alternative for low and medium power applications. Although their thermal properties (i.e., higher thermal resistance per square centimeter) are poorer than those of the ceramic DCB substrates, they are less expensive, more robust, and machinable. The basic structure of an IMS substrate consists of a copper layer for the circuit layout definition, a metal (usually Al) base plate, and a thin thermally conductive dielectric layer between the two metals. This dielectric is usually an epoxy filled with ceramic particles, its thermal conductivity and specific heat being very difficult to know [36]. On top of the substrate are brazed the power semiconductor devices. Wire bonding are reported over the semiconductor dices. Direct measurement of the chip temperature is very difficult (the chip is not always directly accessible, the power circuitry is coupled with the measuring one, etc.) and thermal assessment becomes a complex task. The exact evaluation of power losses requires intrusive and complex techniques. In order to keep as close as possible to the technology of power modules, dynamic heating and cooling experiments are performed in IMS-based test power assemblies, using a dedicated thermal test chip (TTC) as the main experimentation vehicle. This test chip shows the same thermal behavior as typical power devices, but allows simultaneous and decoupled heat generation and temperature sensing.

A. Thermal Test Chip

This device is a 6 mm $\times$ 6 mm silicon chip, 525 μm thick, developed for thermal tests, and assessment of packages and substrates, allowing simultaneous heat dissipation and temperature measurements. It reproduces the thermal behavior of typical vertical power devices, i.e., a heat generation area on top and a vertical heat flux flowing to the heat sink mainly by conduction. The heat is generated by a polysilicon heating resistor distributed on top, while the temperature is measured with a sensing resistor at the chip center. Fig. 4(a) shows the top view of a TTC soldered on a Cu pad, with the required interconnections between the resistors terminals and the external tracks, performed with Al wire bonds. Both resistors are electrically isolated from the silicon substrate by a very thin (30 nm) silicon oxide layer. The thermal resistance of a SiO_2 layer of 6 mm $\times$ 6 mm $\times$ 30 nm is 64×10^{-4} K/W, taking into account a thermal conductivity for this material of 1.3 W/m·K. This means that, for a dissipated power of 52 W, the temperature difference between both oxide surfaces is less than 0.03 K. Consequently, the thermal influence of this layer can be neglected for all practical operation conditions, where the contribution of the other parts of the assembly is more relevant. The heating resistor layout basically consists of 130 parallel polysilicon tracks, 20 μm wide, and spaced by 17.2 μm, thereby presenting a total equivalent resistance value of 60 Ω [36]. Fig. 4(b) shows a partial top view of the TTC surface with a vertical Al pad on the left to connect the parallel polysilicon strips of the heating resistor.

The temperature sensing resistor, visible in Fig. 4(b) and detailed in Fig. 4(c), is implemented with a centered platinum resistor on top of the chip. This sensing resistor is basically a folded Pt track of 700–850 Ω, taking a total area of 700 μm $\times$ 700 μm. The resistance value can be accurately measured using the four-wire technique through the corresponding four Pt pads and wire-bonds. In the zone of the sense resistor, no heat dissipation is produced, and consequently, the temperature at the chip center is slightly lower than in its surrounding area. This temperature difference has been quantified by simulation, and it is around 2 °C for a dissipation of 35 W in steady state. The TTC backside is metalized with the same multilayer used for typical power devices (Ti/Ni/Au in the present case) to allow the same die attach processes and materials, and interface thermal behavior.

B. Test Power Assembly

The analyzed test module includes two TTCs (denoted 9 and 20) attached and connected to an IMS substrate with the same

[1]That is $\widehat{\mathbf{Y}} \to \mathbf{Y}$ when $\varepsilon \to 0$.

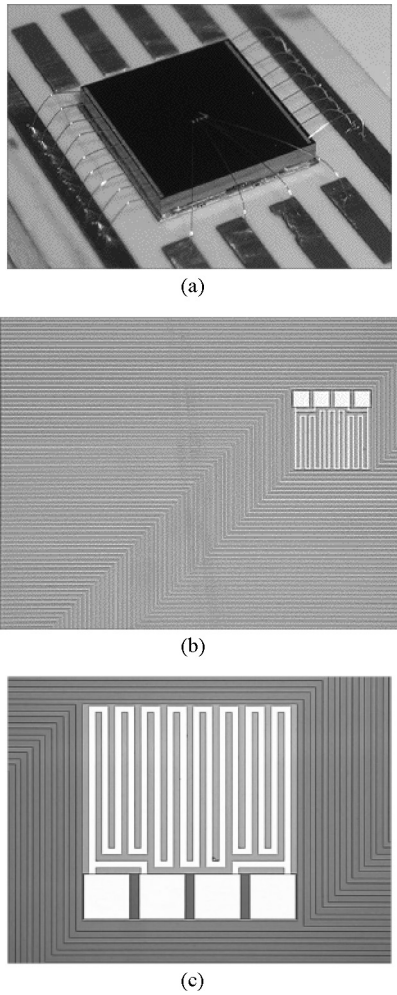

Fig. 4. TTC. (a) TTC soldered on a substrate with the corresponding wire-bonds. (b) Top view of the TTC showing the folded sensing resistor and the heating resistor tracks. (c) Top view detail of the Pt sensing resistor with the four pads for four-wire measurement.

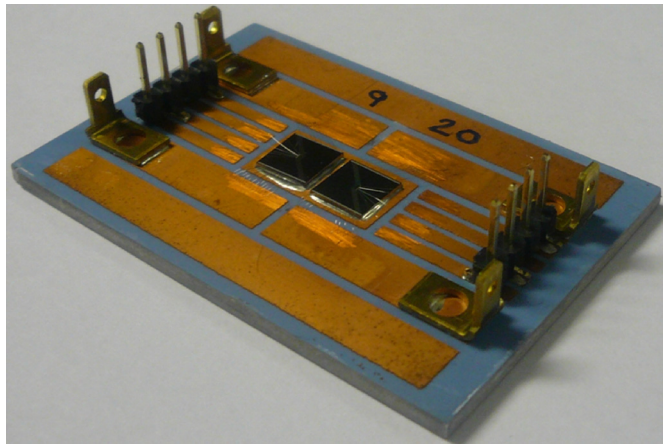

Fig. 5. TTC module as experimental vehicle for this paper.

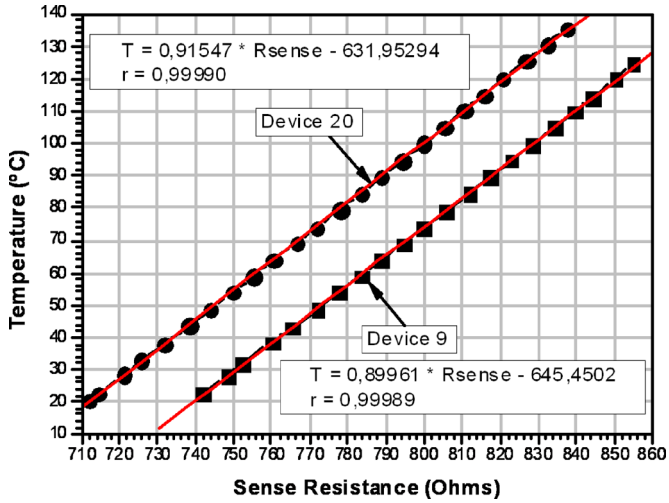

Fig. 6. Calibration of sense resistors in two TTCs with respect to temperature: (dots) experimental data and (lines) linear fit with correlation factors close to 1.

techniques used for true power modules: a soft-solder alloy (SnAgCu) for the die attach and Al wire bonds to connect the resistors pads. Fig. 5 shows a picture of the fabricated test module, showing also the different pins provided to connect the four resistors involved in the measurements to the required external instrumentation. Its lateral dimensions are 52 mm $\times$ 35 mm. The assembly allows the analysis of the self-heating effects as well as the analysis of lateral coupled heating phenomena between chips. In typical applications, power modules are fixed on a heat sink using any kind of thermal interface material (TIM) to improve the thermal contact between the module backside and the heat sink surface. In these conditions, the main heat extraction mechanism is the conduction from the device dissipating area and the heat sink plus convection to ambient environment. Thus, the self-heating phenomena will be dominated by the vertical substrate structure. On the other hand, the lateral heat spreading will depend, apart from the substrate materials, on the layout of the Cu pads and tracks. The most unfavorable thermal coupling will occur between power devices placed on the same Cu pad. To analyze this critical case, the two TTCs of the test assembly have been soldered following this configuration, with a 5-mm gap between them (typical value in power modules).

C. Measurement Setup and Procedure

1) TTC Calibration: A previous calibration step of the sensing resistors is necessary. The test module is placed in an oven, and the sensing resistance of TTCs is measured for temperatures between 20 °C and 135 °C with 5 °C increments. The oven ambient temperature is measured with a PT100 RTD sensor ($\pm$0.1 °C). Fig. 6 shows the corresponding calibration curves for both TTCs. As it can be observed, there is a 30-Ω resistance shift between both chips, although their temperature variation is almost the same.

2) Measurement Setup: Fig. 7(a) shows the measurement scheme for thermal transients. The test module is attached to a forced convection Al heat sink, and their thermal contact is improved with a silicone-based TIM. The heat sink has a small hole allowing the measurement of the reference temperature at the IMS backside center, using a spring loaded K-type thermo-couple. A power switch [insulated-gate bipolar

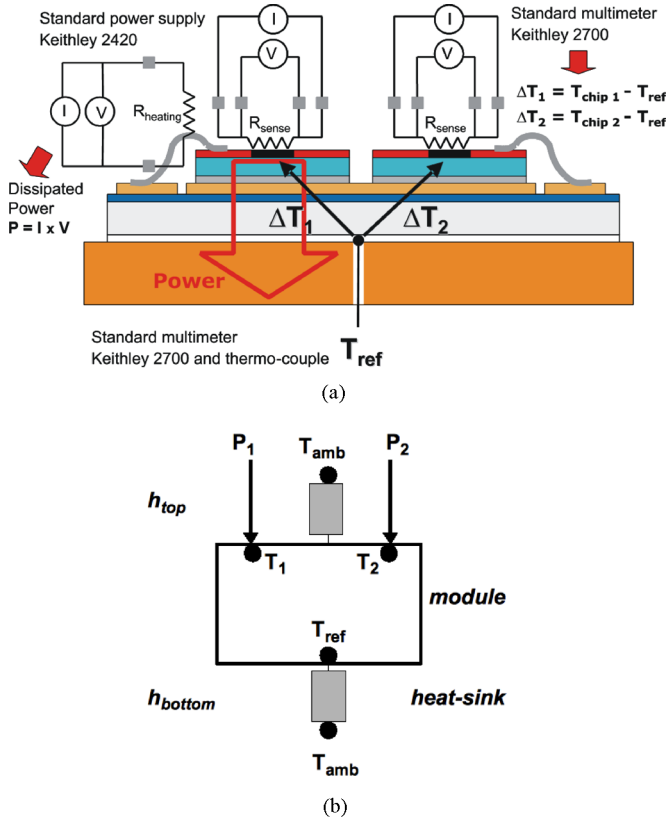

Fig. 7. (a) Measurement scheme for thermal transients. (b) Symbolic view considered for modeling.

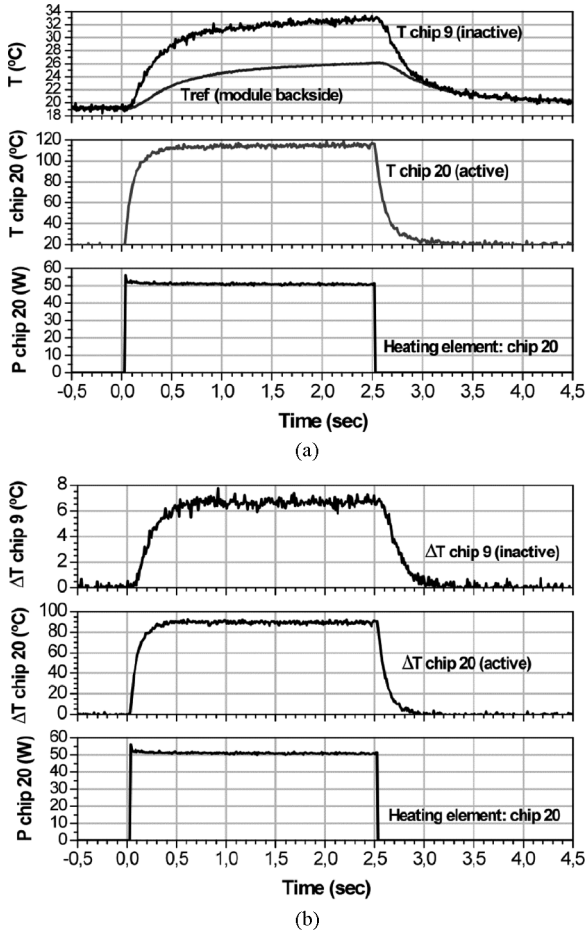

Fig. 8. Experimental waveforms for 52 W, 2.5 s power pulse applied to a TTC. (a) Direct measurement. (b) Correction of module backside temperature.

transistor (IGBT)] is used to apply a voltage pulse to the heating resistor from a dc power supply (Keithley 2420).

The pulse duration is determined from a waveform generator, and the control signal is applied to the IGBT through a gate drive circuit [not represented in Fig. 7(a)]. A source measure unit (Keithley 2410) is used as current source to inject a sensing current into the sensing resistor. The chip temperature is derived from the voltage drop waveform across the sensing resistor and the corresponding calibration curve. Finally, the time evolution of the module backside temperature (reference temperature) is acquired from an instrumentation amplifier based on the AD595 IC, which translates the thermocouple signal to a higher voltage level easily measured with the oscilloscope. Although the nominal IC output gives a 10 mV/°C signal, the $T_{\rm ref}$ measurement chain is calibrated to obtain more accurate results. In addition, this calibration is performed using the same PT100 sensor used previously for the calibration of the TTC sensing resistors. This allows the reduction of the error of the temperature difference between the chips and the reference.

Fig. 8(a) shows the different waveforms measured for a 52 W/2.5 s power pulse applied to one of the TTCs (named 20) with a 100-Hz sampling rate. As it can be observed, the power waveform shows a slight overshoot at the initial time due to the increase of the polysilicon heating resistance value with temperature. This variation has been approximately evaluated to 0.05 Ω/K. The ambient air temperature being 19 °C, the active device reaches 118 °C, and the module backside 26 °C.

Another important aspect that can be observed in Fig. 8 is that after 2.5 s, the temperatures have not reached their steady-state values. In fact, at this moment, the heat sink is still increasing its temperature under the influence of the thermal interface material between its surface and the module backside. To analyze only the thermal behavior of the test module and for the sake of reproducible measurements, i.e., independent of BCs due to the environment, the differences between the chip temperatures and the reference temperature are then evaluated, as shown in Fig. 8(b). The measurement procedure gives access to absolute temperatures, i.e., including the BCs effect over the module, or temperature differences, i.e., independent of the BCs imposed by the environment through the thermal behavior of the heat sink. The top interface is protected by an insulator layer that behaves like a thermal insulator even in the case of heat dissipation of several seconds.

A compact thermal model is now constructed for the TTC assemblies, identified, and validated.

D. Model Identification

As shown in Fig. 7, a one-input/one-output thermal model is first considered for each TTC device. The input is the power losses, P, injected as heat into the assembly (that mimics a

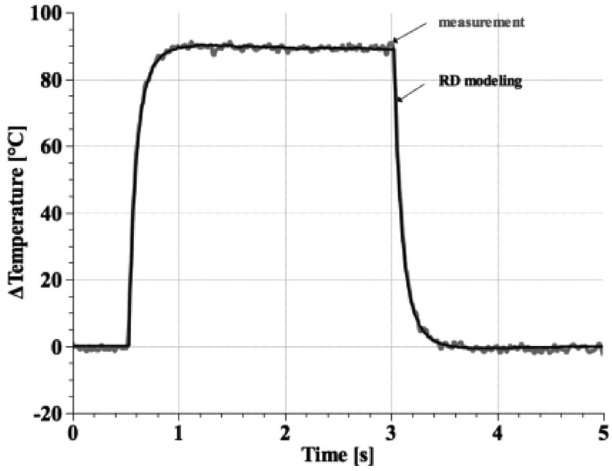

Fig. 9. Thermal response of TTC 20 to a power pulse of 52 W, 2.5 s.

power module), and the output is the silicon temperature in the center of the silicon die, T_j. This temperature mimics a so-called junction temperature. The discretized DR model (18) requires the identification of the state-space model order, N, the frequency base, ξ, and the diffusive symbol, η

$$\begin{cases} \dfrac{d\psi_k}{dt} = -\xi_k \psi_k(t) + P(t) \text{ with} \\ \psi_k(0) = 0, \qquad \text{for } 1 \le k \le N \\ T_j(t) = \displaystyle\sum_{k=1}^{N} \eta_k \psi_k(t). \end{cases} \tag{18}$$

The frequency mesh, ξ, corresponds to the time horizon of the analyses for which the model is pertinent. As stated in Section I, the diffusion of heat inside the system stimulates a thermal system that changes with time as different thermal interfaces and layers are touched by the heat propagation. The challenge of model reduction in published methods is to reduce an initial model, valid for short- and long-duration heat injections, to a more compact model when a specific time horizon analysis is selected. DR works the other way round: the time horizon of the model validity is first selected, and then, the model parameters are identified from an accurate simulation result or a pertinent experimental response.

In the case of an identification from an experimental result, the time resolution is limited by the data sampling rate. If a long-term thermal response is considered, then the amount of data is large. It is the main reason for considering a logarithmic timescale in [18] and [12], as the authors need to differentiate the short-term and long-term thermal responses.

TTC device 20 in Fig. 5 is stimulated by a power pulse of 52 W during 2.5 s. The thermal response is evaluated (see Fig. 9) and used as identification data. The state-space model order, N, the frequency base, ξ, and the diffusive symbol, η, are identified using the rule of thumb and identification procedure detailed in Section II. The data sampling rate is $t_{\text{sample}} = 10$ ms, and a rough time constant of $\tau = 0.5$ s can be estimated during the heating edge. The minimum value of the frequency range is set to $\xi_0 = 1.8$ rad·s$^{-1} \le 1/\tau$ and the maximum value is set to $\xi_6 = 1000$ rad·s$^{-1} \ge 1/t_{\text{sample}}$. The heuristic rule of thumb to set the system order is to count the number of thermal interfaces between the location of heat injection and the location of the reference temperature (7 as pictured in Fig. 7). The frequency mesh, ξ, is set as a geometric sequence of ratio $r = 2.8672$ in the present case. As explained in Section II, the diffusive symbol, η, is obtained by least-square optimization between the simulation and the input data [see Table I and Fig. 10(a)]. If the response is not satisfying, the identification procedure must be performed again increasing the system order. The experience of the authors is that the heuristic rule for system-order evaluation has not been defeated so far.

TABLE I
IDENTIFIED PARAMETERS OF THE THERMAL MODEL (18) WITH DATA IN FIG. 9

	$\xi, rd.s^{-1}$	$\eta, K.(W.s)^{-1}$
0	1,8	0,38
1	5,16	1,02
2	14,8	23,0
3	42,4	-21,07
4	121,6	165,9
5	348,8	-2336,6
6	1000	5785,2

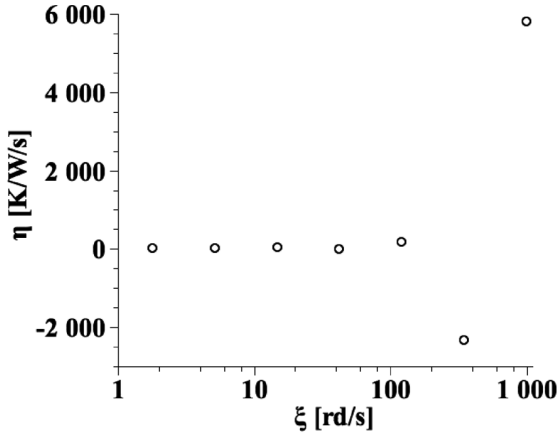

(a)

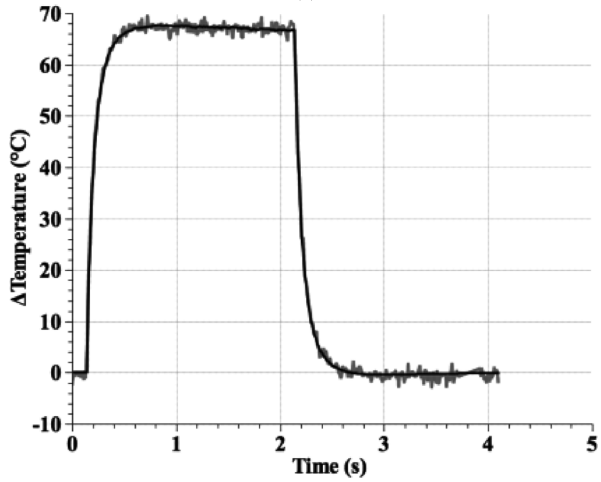

(b)

Fig. 10. (a) DR model parameter and (b) validation of the identified thermal model under (41.5 W, 2 s) power pulse.

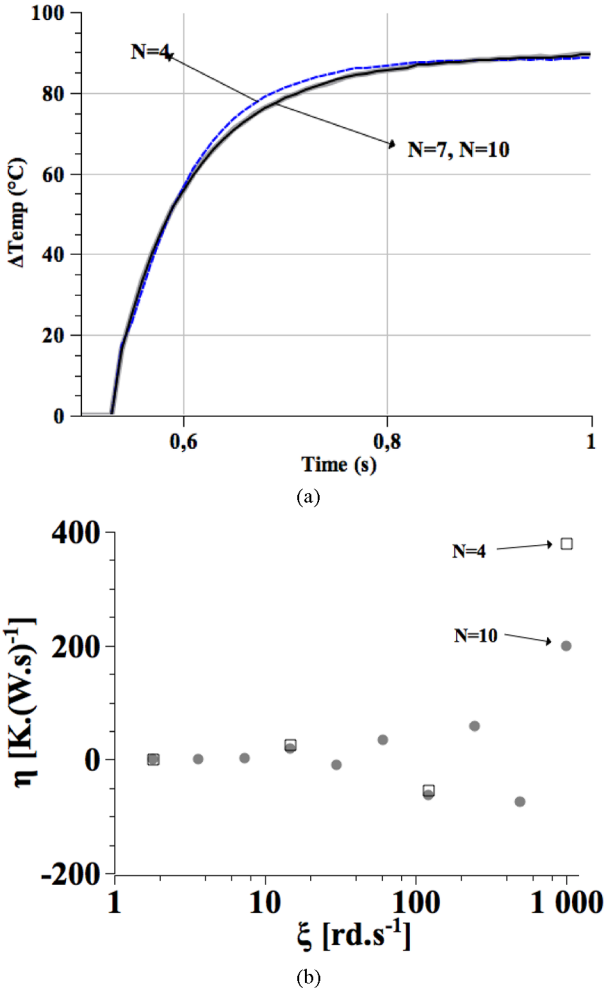

Fig. 11. (a) Simulation of thermal response of TTC 20 model to a power pulse of 52 W, 2.5 s, and identified with order 4, 7, and 10, respectively (optimal is $N = 7$, Fig. 9). (b) Parameters of the identified models of order 4 and 10, respectively.

The model in (18) may be implemented easily using a hardware-description language or popular software like MATLAB. Appendix gives a VHDL-AMS description with the parameters in Table I. The simulation of the thermal model is shown in Fig. 9. The identified model is validated using different power pulse conditions. Fig. 10(b) shows a comparison with experimental measurements for a power pulse of 41.2 W and 2 s and a good agreement is obtained.

The thermal response of TTC 20 to a power pulse of 50 W, 2.5 s (see Fig. 9) is identified for a system order less than the optimal value ($N = 4$) and larger than the optimal value ($N = 7$ and $N = 10$). It is obvious from Fig. 11(a) that the response is not represented correctly if the frequency mesh is too small and the accuracy is not improved if the frequency mesh is increased in size. For an optimal model order, the accuracy is limited by the time resolution of the identification input data and the time horizon validity given to the model. Fig. 11(b) represents the parameters of the identified models for order 4 and 10, respectively. The identified parameters of the optimal-order model are shown in Fig. 10(a). Various frequency values are very close between the different frequency meshes and the

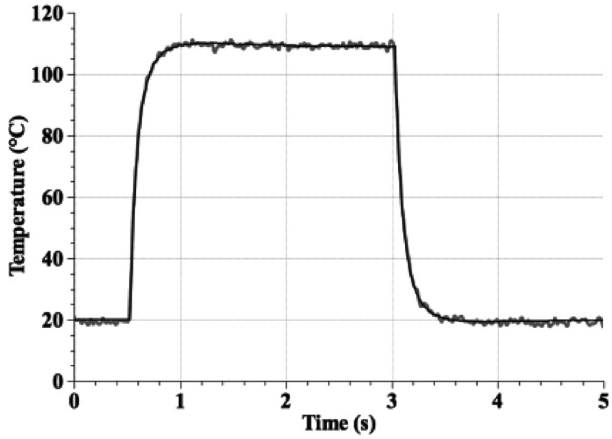

Fig. 12. Thermal response of TTC 20 to a power pulse of 52 W, 2.5 s: absolute temperature.

associated diffusive symbols also. The frequency mesh and the diffusive symbols do not have the signification of eigenvalues, but it may be seen that the identification procedure acts like a model reduction routine as "points" are removed when the model order is decreased. Moreover, like in a model reduction routine, the model accuracy decreases with the model order, but without a sharp change as the frequency mesh is always set optimally and the diffusive symbols are identified using a least-square optimization.

The model has been identified using the module backside temperature as the reference temperature. This measurement method avoids the influence of the heat sink and the environment [see Fig. 7(b)]. The model is then independent of the BCs in the way that only convection appears inside the module. The BCs are added to the BC-independent model, similarly as in [18], to obtain the full thermal model. In the case of the experimental vehicle and static BCs, the heat sink and the environment are replaced by effective heat transfer coefficients, $h_{\mathrm{top}} = 6.0\ \mathrm{W{\cdot}(K{\cdot}m^2)^{-1}}$ and $h_{\mathrm{bottom}} = 22.5\ \mathrm{W{\cdot}(K{\cdot}m^2)^{-1}}$ (heat sink of 24 cm^2 and effective 0.54 W/K), identified from the thermal response of Fig. 9. The absolute temperature of TTC 20 is shown in Fig. 12, and a good agreement is obtained. Time-dependent BCs must be represented by adequate models, as in [18].

IV. Two-Inputs/Two-Outputs Model

The vehicle in Fig. 5 is now used to illustrate the construction, identification and validation of the thermal model of a coupling between two heat sources. This is the common situation in a power module where multiple power devices are soldered on the same substrate within small distance.

A. Identification From Experimental Data

The thermal model has two inputs (the power generated by each source, i.e., TTC9 and TTC20) and two outputs (the source temperatures). As aforementioned, the temperatures are considered with respect to the reference temperature in order to produce a BC-independent thermal model. The linearity assumption enables to build the thermal model by parts (see Section III-C.2).

A state-space representation takes care of the contribution of the thermal system to the temperature of one device (TTC20) when it is generating heat and the other device (TTC9) is passive (19). A state-space representation takes care of the passive device temperature under influence of the other device heat generation (20). Inversing the role of the devices yield (21) and (22). Finally, the device temperature, respectively, T_9 and T_{20}, is obtained by combination of the contributions (23)

$$\begin{cases} \text{self-heating in TTC 20 when active and TTC 9 passive} \\ \dfrac{d\psi_k}{dt} = -\xi_k \psi_k(t) + P_1(t) \text{ with} \\ \psi_k(0) = 0, \qquad \text{for } 1 \le k \le N_1 \end{cases} \tag{19}$$

$$\begin{cases} \text{heating in TTC 9 when TTC 20 active and TTC 9 passive} \\ \dfrac{d\zeta_k}{dt} = -\nu_k \zeta_k(t) + P_1(t) \text{ with} \\ \zeta_k(0) = 0, \qquad \text{for } 1 \le k \le N_2 \end{cases} \tag{20}$$

$$\begin{cases} \text{self-heating in TTC 9 when active and TTC 20 passive} \\ \dfrac{d\beta_k}{dt} = -\omega_k \beta_k(t) + P_2(t) \text{ with} \\ \beta_k(0) = 0, \qquad \text{for } 1 \le k \le N_3 \end{cases} \tag{21}$$

$$\begin{cases} \text{heating in TTC 20 when TTC 9 active and TTC 20 passive} \\ \dfrac{d\alpha_k}{dt} = -\lambda_k \alpha_k(t) + P_2(t) \text{ with} \\ \alpha_k(0) = 0, \qquad \text{for } 1 \le k \le N_4 \end{cases} \tag{22}$$

$$\begin{cases} T_{20}(t) = \displaystyle\sum_{k=1}^{N_1} \eta_{1k} \psi_k(t) + \sum_{k=1}^{N_4} \eta_{4k} \alpha_k(t) \\ T_9(t) = \displaystyle\sum_{k=1}^{N_2} \eta_{2k} \zeta_k(t) + \sum_{k=1}^{N_3} \eta_{3k} \beta_k(t). \end{cases} \tag{23}$$

The model identification requires two tests where one TTC is active and the other passive, and *vice versa*. Both device temperature responses are recorded and the parameters, (ξ_k, η_{1k})–(λ_k, η_{4k}), are identified. The state-space systems should have the same order as quite the same physical thermal system is stimulated with respect to TTC20 and TTC9. However, it could happen that a significant difference in thermal coupling enables one to choose a system order slightly smaller than the other one. As the TTC devices in the experimental module are similar, it is normal to find identical order for the four state-space representations. The frequency mesh, ξ, is set identical for self-heating and coupling effects. One set of diffusive symbols, η_a, is to be identified for self-heating effects and another one, η_b, for couplings effects. Moreover, as only two similar devices are involved, the thermal models of self-heating and thermal couplings are consequently similar. In most cases, symmetry does not apply and as many parameter identifications are required as necessary dataset to cover all possible couplings inside the system.

TTC20 is stimulated with a power pulse of 50 W during 0.5 s when TTC9 is passive [see Fig. 13(a)]. TTC9 is stimulated with a power pulse of 40 W during 500 ms when TTC20 is passive. Table II lists the parameters of the self-heating and coupling parts of the DR model. The coupling model is of order 6, whereas self-heating is previously identified for order 7. First,

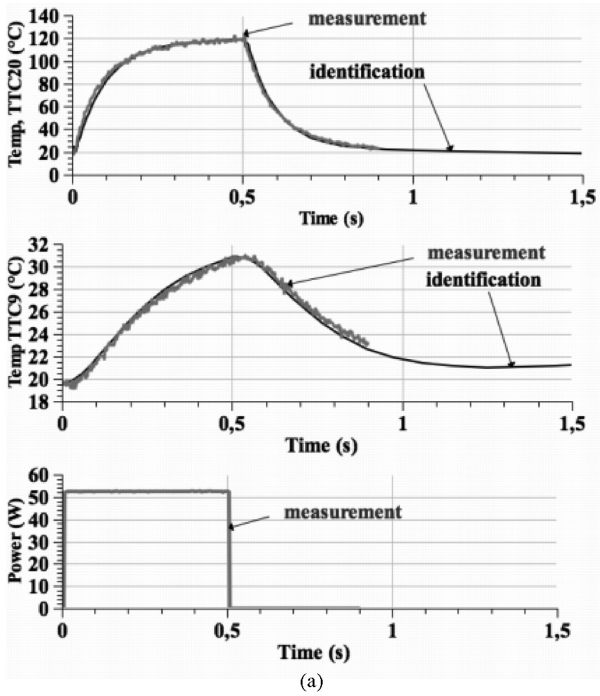

(a)

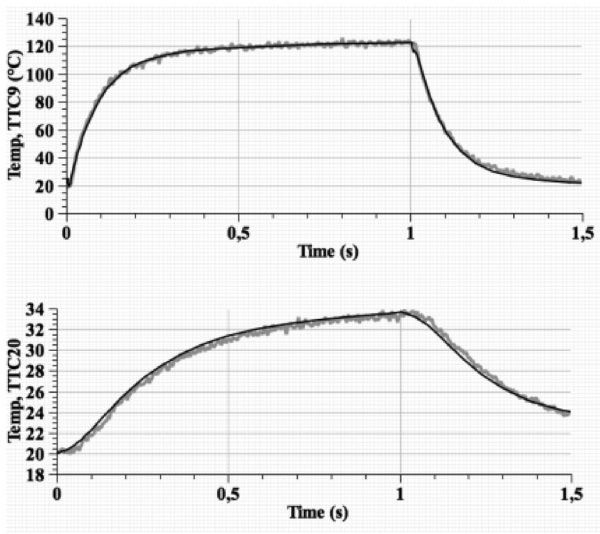

(b)

Fig. 13. (a) Dataset for identification of DR thermal model, 50 W/0.5 s power pulse on TTC20, TTC9 passive. (b) Validation of the thermal model (50 W/1 s) power pulse on TTC9, TTC20 passive.

TABLE II
IDENTIFIED PARAMETERS OF THE THERMAL MODELS FOR SELF-HEATING AND COUPLINGS

$\xi, rd.s^{-1}$	$\eta_a, K.(W.s)^{-1}$	$\eta_b, K.(W.s)^{-1}$
0,2	-0,08	0,3
1,57	0,63	-0,55
12,36	23,45	9,2
97,12	-4,7	-1,9
763,3	-627,6	77
5000	4312,5	932

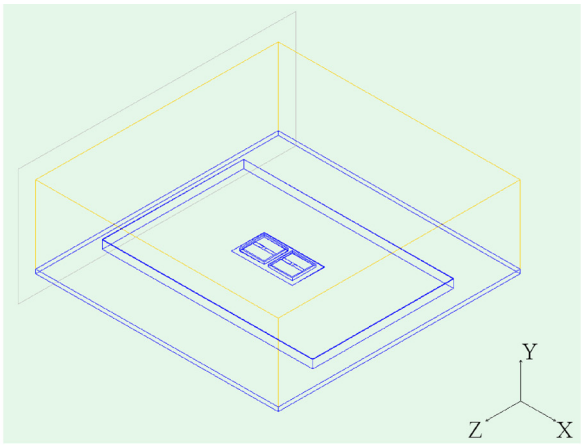

(a)

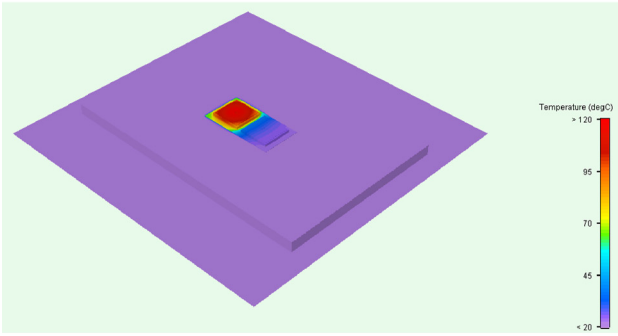

(b)

Fig. 14. (a) Description of test chip using FLOTHERM. (b) Typical simulated temperature field when one chip is active.

the identification of DR model is iterative, starting from a guess value for the system order (rule of thumb in the case of self-heating). Second, the identification must be performed with input data related to the targeted time horizon of the model validity. Table I is related to input data correlated to a power pulse of 2.5 s. Table II is related to input data correlated to a power pulse of 0.5 s. The small change in model order is then not surprising. The two-input/two-output model could have been identified for an order of 7 or more without change in accuracy [see Fig. 11(a)]. The time horizon of the model validity is not increased with larger model order, but depends on input data characteristics.

Fig. 13(b) shows one case of validation. The identified model is simulated when the device TTC9 is stimulated with a power pulse of 50 W during 1 s, and the device TTC20 is passive.

B. Identification from Simulation Data

To illustrate the usefulness of compact models constructed by DR, fine 3-D thermal simulations of the test power module previously described have been performed using FLOTHERM [37]. This computational fluid dynamics (CFD) software is based on finite differences and rectangular grid cells. The module model shown in Fig. 14(a) has been considered over a bottom isothermal surface at 20 C representing the heat sink. The temperature differences between the chips and the substrate backside are

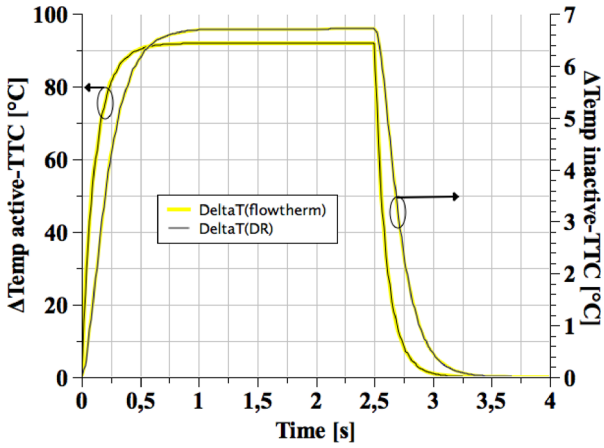

Fig. 15. Comparison of simulated thermal response of the test chip in Fig. 14(a) using FLOTHERM and a DR model identified from FLOTHERM prior simulations: one TTC is stimulated (52 W, 2.5 s) and the other one is passive.

analyzed with test points placed at these locations. In prior simulations, it has been verified that for normal operating conditions, only heat conduction mechanisms are relevant, and the air volume over the assembly can be considerably reduced to minimize the number of grid points and the importance of convection phenomena. The thermal parameters (thermal conductivity and specific heat) of the involved materials (Cu, SiO_2, Al, etc.) have been considered constant, except for the thermal conductivity of Si. Besides the composition of IMS, dielectric layer has been considered with 60% of Al_2O_3 particles and 40% of epoxy resin. Most thermal conductivities have been extracted and other thermal properties values in the literature have been thoroughly verified. Finally, 50 ms steps are used during the rising and falling edges of the applied power pulse, while 100 ms steps are used during the slower dynamic phases. Fig. 14(b) shows the typical simulated surface temperature field when one TTC is active and the other inactive. Four similar simulations are needed to identify the DR model (tenth order). Thermal responses in the range of seconds have been considered. Fig. 15 shows a comparison when one TTC is stimulated with 52 W during 2.5 s and the other TTC is inactive. The DR model gives a result within a second and FLOTHERM necessitates 20 min computation. The comparison demonstrates a good agreement and the pertinence of numerical simulations to provide input data to DR model identification. This allows to mix the approaches in the frame of virtual prototyping of power conversion systems.

V. Discussion

DR aims to build a state-space representation of a thermal system from behavioral viewpoint. BCs may be included in the model development or not, as in [18]. In contrary to [7], [12], or [18], DR does not need a geometric and material description of the system. However, if this description is available, it is possible to build a BC-independent model. One interest of DR is to build a behavioral compact model of a system, including BCs. It is demonstrated in [38] how to produce a successful

compact electrothermal model to evaluate the peak temperature of an IGBT die soldered on a DCB substrate and under short-circuit operation.

Another advantage of DR is to control the frequency bandwidth or time horizon validity of the model. It means that the user defines *a priori* the time horizon validity of the model with respect to the virtual prototyping analysis to be performed, as many models as analyses may be necessary depending on the required time resolution. Model reduction acts differently as it starts from the most accurate representation and yields reduced time-resolution models. Model reduction and diffusive model identification require almost the same computation effort as they manipulate data of similar size. Finally, a systematic study should be carried out to confront the reduction efficiency obtained by diffusive model identification or Krylov subspace method for example.

The size of the reduced models may still be very large in the case of *RC*-networks, Foster or Cauer as well. If a linear geometric meshing is considered (centered finite-difference scheme, for example), then huge *RC*-networks remain. Considering a simple thermal problem in [39] and [40], it has been demonstrated that a 1000 *RC*-cell model was required to obtain results of equivalent accuracy as those obtained with a 26th-order FEM or a fifth-order DR model for the same thermal problem. The large amount of *RC*-networks comes from a linear discretization of the geometry where the thin step value is dictated by the targeted accuracy (maximal temperature rise close to the surface). A nonlinear geometric discretization leads to an order of 100 *RC*-cells, but generally, a reduction method must be employed. Finite elements are not truly the best option, in general (the most accurate solution), for electrical or thermal problems: finite volumes (or boundary methods) may perform just as well or even better. The order of the FEM model may be slightly reduced with a refinement in meshing, but remains larger than the DR model order. The issue is then not the accuracy or the complexity to build the model, but the final order of the thermal model plus the possibility for the user to control the accuracy and time horizon validity of the thermal model.

If a logarithmic timescale is adopted, then the *RC*-network size is also significantly reduced, but the data manipulation is delicate and the model cannot be used easily with a circuit simulator [12].

DR, as presented here, is not able to construct geometry-dependent models. Published methods in literature show the same limitation except exploratory works like [15]. It has been demonstrated that the formal construction of the compact model from the geometric description of the system is limited to regular and simple shapes [29]. Building the compact model from a simplification of the system description as in [15] is not worth the effort due to a limited model accuracy. So, the geometric optimization of a system within virtual prototyping requires the diffusive model to be constructed every nth iterations of the optimization routine depending on the required accuracy. If the system geometry is managed by a mesh-based software, simulation may be used to produce the necessary data for the identification of the compact model.

VI. Conclusion

DR has been introduced as a formal method to build a compact state-space thermal model of a system in a behavioral manner. BCs may be included or not, depending on the objectives of the analysis that uses the thermal model.

Theoretically, the method is dedicated to the representation of nonrational system based on infinite contributions. A discrete formulation of the DR yields a practical engineering modeling method. The identification routine is efficient and accommodates experimental or simulation results as input data. DR enables to model a given system, provided that the temperature to be monitored is observable for the purpose of prior identification. It can be a physical or virtual system. The model is then global and behavioral, but dependent on BCs. In the frame of virtual prototyping, DR applies to the current design of the system to produce a compact model for expensive investigations like control or stress. DR model is not currently adequate for the system geometric optimization.

It has been shown that the frequency bandwidth or the time horizon validity of the model can be controlled during the identification step. Unlike most published methods, the compact model comes directly from identification and no reduction step is necessary afterward. The authors' experience is that the identification routine produces compact models of the similar order as the Krylov subspace method, but with a more explicit input of the user as he controls the frequency meshing.

DR has been applied to the representation of thermal couplings and the agreement with experiment is very good. Future work concerns an extensive comparison of the DR method with existing numerical methods, reduction methods, and published compact modeling methods based on a complex electrothermal problem. Theoretical developments concern geometry-dependent DR.

Appendix

VHDL-AMS Implementation of a DR Model

```
LIBRARY ieee;
USE ieee.thermal_systems.ALL;
USE ieee.math_real.ALL;
– ENTITY DECLARATION thermal_system –
ENTITY thermal_system IS
PORT (TERMINAL tt : thermal);
END ENTITY thermal_system;
– ARCHITECTURE DECLARATION arch_DR –
ARCHITECTURE arch_DR OF thermal_system IS
CONSTANT T0 : real := 298.15; –amb. temp [K]
CONSTANT R : real := 2.8672; – model param
CONSTANT xsimin : real := 1.8; – model param
– Free quantities: State Variables –
QUANTITY F0 : real := 0.0;
QUANTITY F1 : real := 0.0;
QUANTITY F2 : real := 0.0;
QUANTITY F3 : real := 0.0;
QUANTITY F4 : real := 0.0;
QUANTITY F5 : real := 0.0;
```

```
QUANTITY F6 : real := 0.0;
QUANTITY deltaTemp: real := 0.0;
QUANTITY Tj ACROSS Pth THROUGH tt TO thermal_ref;
BEGIN
–State variable equations
F0'dot == -(xsimin)*F0+Pth; –Pth, dissipated power
F1'dot == -(R*xsimin)*F1+Pth;
F2'dot == -(R*R*xsimin)*F2+Pth;
F3'dot == -(R*R*R*xsimin)*F3+Pth;
F4'dot == -(R*R*R*R*xsimin)*F4+Pth;
F5'dot == -(R*R*R*R*R*xsimin)*F5+Pth;
F6'dot == -(R*R*R*R*R*Rxsimin)*F6+Pth;
– Monitored Temperature, transient thermal response
deltaTemp == 0.38*F0+1.02*F1+23.0*F2
-21.07*F3+165.9*F4-2336.6*F5+5785.2*F6;
Tj == deltaTemp+T0;
END ARCHITECTURE arch_DR;
```

REFERENCES

[1] L. Seung-Yo, A. G. Pfaelzer, and J. D. V. Wyk, "Comparison of different designs of a 42V/14V DC/DC converter regarding losses and thermal aspects," *IEEE Trans. Ind. Appl.*, vol. 43, no. 1, pp. 520–530, Mar./Apr. 2007.

[2] M. Sabry, "Dynamic compact thermal models used for electronic design: A review of recent progress," in *Proc. Int. Electron. Packag. Tech. Conf. Exhib. (IPACK)*, 2003, pp. 1–17.

[3] M. Rencz and V. Szekely, "Studies on the nonlinearity effects in dynamic compact model generation of packages," *IEEE Trans. Compon. Packag. Technol.*, vol. 27, no. 1, pp. 124–130, Mar. 2004.

[4] F. Christiaens, B. Vandevelde, E. Beyne, R. Mertens, and J. Berghmans, "Generic methodology for deriving compact dynamic thermal models applied to PSGA packages," *IEEE Trans. Compon. Packag., Manuf. Technol.*, vol. 21, no. 4, pp. 565–576, Dec. 1998.

[5] D. Schweitzer and H. Pape, "Boundary condition independent dynamic thermal compact models of IC-packages," in *Proc. 9th THERMINIC*, 2003, pp. 225–230.

[6] D. Celo, X. M. Guo, P. K. Gunupudi, R. Khazaka, D. J. Walkey, T. Smy, and M. S. Nakhla, "Hierarchical thermal analysis of large IC modules," *IEEE Trans. Compon. Packag. Technol.*, vol. 28, no. 2, pp. 207–217, Jun. 2005.

[7] M. Rencz and V. Szekely, "Dynamic thermal multiport modeling of IC packages," *IEEE Trans. Compon. Packag. Technol.*, vol. 24, no. 4, pp. 596–604, Dec. 2001.

[8] G. Wachutka, "Modeling of miniaturized electro-thermo-mechanical systems using thermodynamic methods," *Micromech. Sens., Actuators Syst.*, vol. 40, pp. 183–197, 1992.

[9] T. Bechtold, J. G. Korvink, and E. B. Rudnyi, *Fast Simulation of Electro-Thermal MEMS: Efficient Dynamic Compact Models*. New York: Springer-Springer, 2007.

[10] T. Kojima, Y. Yamada, Y. Nishibe, and K. Torii, "Novel RC compact thermal model of HV inverter module for electro-thermal coupling simulation," in *Proc. IEEE Power Convers. Conf. (PCC)*, 2007, pp. 1025–1029.

[11] J. Palacin, M. Salleras, J. Samitier, and S. Marco, "Dynamic compact thermal models with multiple power sources: Application to an ultrathin chip stacking technology," *IEEE Trans. Adv. Packag.*, vol. 28, no. 4, pp. 694–703, Nov. 2005.

[12] D. Li, S. X.-D. Tan, and M. Tirumala, "Architecture-level thermal behavioral characterization for multi-core processors," in *Proc. IEEE Asian South-Pacific Des. Autom. Conf. (ASPDAC)*, 2008, pp. 456–461.

[13] M. Rencz, A. Poppe, E. Kollar, S. Ress, and V. Szekely, "Increasing the accuracy of structure function based thermal material parameter measurements," *IEEE Trans. Compon. Packag. Technol.*, vol. 28, no. 1, pp. 51–57, Mar. 2005.

[14] M. Rencz, V. Szekely, and A. Poppe, "A methodology for the co-simulation of dynamic compact models of packages with the detailed models of boards," *IEEE Trans. Compon. Packag. Technol.*, vol. 30, no. 3, pp. 367–374, Sep. 2007.

[15] J. Ortiz-Rodriguez, A. R. Hefner, D. Berning, M. Velez-Reyes, M. Hernandez-Mora, and J. Gonzalez, "Lumped-parameter thermal modeling of an IPEM using thermal component models," in *Proc. IEEE PESC*, 2004, pp. 43–48.

[16] L. Vu-Quoc, Y. Zhai, and K. D. T. Ngo, "Efficient simulation of coupled circuit-field problems: Generalized Falk method," *IEEE Trans. Comput.-Aided Des. Integr. Circuits Syst.*, vol. 23, no. 8, pp. 1209–1219, Aug. 2004.

[17] D. Celo, X. Guo, P. K. Gunupudi, R. Khazaka, D. J. Walkey, T. Smy, and M. S. Nakhla, "The creation of compact thermal models of electronic components using model reduction," *IEEE Trans. Adv. Packag.*, vol. 28, no. 2, pp. 240–251, May 2005.

[18] Y. C. Gerstenmaier, A. Castellazzi, and G. K. M. Wachutka, "Electrothermal simulation of multichip-modules with novel transient thermal model and time-dependent boundary conditions," *IEEE Trans. Power Electron.*, vol. 21, no. 1, pp. 45–55, Jan. 2006.

[19] Y. Iwata, S. Hayashi, and K. Fujimoto, "An efficient thermal design method based on boundary condition modeling," *IEEE Trans. Compon. Packag. Technol.*, vol. 29, no. 3, pp. 594–603, Sep. 2006.

[20] C. J. M. Lasance, "Recent progress in compact thermal models," in *Proc. 19th IEEE SEMI-THERM Symp.*, 2003, pp. 290–299.

[21] L. T. Pillage and R. A. Rohrer, "Asymptotic waveform evaluation for timing analysis," *IEEE Trans. Comput.-Aided. Des.*, vol. 9, no. 4, pp. 352–366, Apr. 1990.

[22] L. Codecasa, D. D'Amore, and P. Maffezzoni, "An Arnoldi based thermal network reduction method for electro-thermal analysis," *IEEE Trans. Compon. Packag. Technol.*, vol. 26, no. 1, pp. 186–192, Mar. 2003.

[23] Y. C. Liang, H. P. Lee, S. P. Lim, W. Z. Lin, K. H. Lee, and C. G. Wu, "Proper orthogonal decomposition and its applications—Part I: Theory," *J. Sound Vib.*, vol. 252, no. 3, pp. 527–544, 2002.

[24] K. Willcox and A. Megretski, "Fourier series for accurate, stable, reduced-order models for linear CFD applications," in *Proc. 16th AIAA Comput. Fluid Dyn. Conf.*, 2003, pp. 2003–4235.

[25] Y. C. Gerstenmaier and G. Wachutka, "Dependent temperature fields calculated using eignefunctions and eignevalues of the heat conduction equation," *Microelectron. J. Sound Vib.*, vol. 32, pp. 801–808, 2001.

[26] S. X.-D. Tan, *Advanced Model Order Reduction Techniques in VLS Design*. Cambridge, U.K.: Cambridge Univ. Press, 2007.

[27] M. Salleras, T. Bechtold, L. Fonseca, J. Santander, E. B. Rudnyi, J. G. Korvink, and S. Marco, "Comparison of model order reduction methodologies for thermal problems," in *Proc. 6th Int. Conf. Therm., Mech. Multi-Phys. Simulation Exp. Micro-Electron. Micro-Syst., 2005 (EuroSimE 2005)*, Apr., pp. 60–65.

[28] P. Bidan, T. Lebey, G. Montseny, C. Neacsu, and J. Saint-Michel, "Transient voltage distribution in inverter fed motor windings: Experimental study and modeling," *IEEE Trans. Power Electron.*, vol. 16, no. 1, pp. 92–100, Jan. 2001.

[29] L. Laudebat, P. Bidan, and G. Montseny, "Modeling and optimal identification of pseudodifferential electrical dynamics by means of diffusive representation—Part I: Modeling," *IEEE Trans. Circuits Syst.*, vol. 1, no. 1, pp. 1–13, Sep. 2004.

[30] A. Rumeau, P. Bidan, T. Lebey, L. Marchin, B. Barbier, and S. Guillemet, "Behavior modeling of a $CaCu_3Ti_4O_{12}$ ceramic for capacitor applications," in *Proc. IEEE Conf. Electr. Insul. Dielectr. Phenom.*, 2006, pp. 23–26.

[31] K. B. Smida, P. Bidan, T. Lebey, F. B. Ammar, and M. Elleuch, "Identification and time-domain simulation of the association inverter-cable-asynchronous machine using diffusive representation," *IEEE Trans. Ind. Electron.*, vol. 56, no. 1, pp. 257–265, Jan. 2009.

[32] G. Montseny, J. Audounet, and B. Mbodge, "Optimal models of fractional integrators and application to systems with fading memory," in *Proc. IEEE Int. Conf. Syst., Man Cybern.*, 1993, pp. 65–70.

[33] G. Monstseny, "Diffusive representation of pseudodifferential time-operators," *Proc. ESAIM*, vol. 5, pp. 159–175, 1998.

[34] G. Monstseny, "Diffusive representation: A new concept for complex dynamic problems involving pseudo differential operators," in *Lecture Notes of the Summer School "On the Links Between Nonlinear Physics and Information Sciences"*. France: Les Houches Center of Physics, 2002.

[35] G. Montseny. (2001). Pseudo differential operators and diffusive representation in modeling, control and signal, LAAS, France, Tech. Rep. [Online]. Available: http://www.laas.fr/gt-opd/opdrd-en/index.html.en

[36] X. Jorda, X. Perpina, M. Vellvehi, and J. Coleto, "Power-substrate static thermal characterization based on a test chip," *IEEE Trans. Device Mater. Rel.*, vol. 8, no. 4, pp. 671–679, Dec. 2008.

[37] *Flotherm User Manual*, Version 6.1 ed., Flomerics Limited, Surrey, U.K., 2005.
[38] S. M'rad, B. Allard, X. Jorda, and M. Vellvehi, "An experimentally verified compact transient electro-thermal modeling procedure for power modules," in *Proc. Power Electron. Appl., 2007 Eur. Conf.*, Aalborg, Denmark, Sep., pp. 1–8.
[39] A. Ammous, B. Allard, and H. Morel, "Transient temperature measurement and modeling of IGBTs under short circuit," *IEEE Trans. Power Electron.*, vol. 13, no. 1, pp. 12–25, Jan. 1998.
[40] A. Ammous, K. Ammous, H. Morel, B. Allard, D. Bergogne, and F. Sellami, "Electrothermal modeling of IGBTs: Application to short-circuit conditions," *IEEE Trans. Power Electron.*, vol. 15, no. 4, pp. 778–789, Jul. 2000.

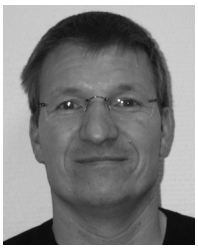

Bruno Allard (M'93–SM'02) was born in 1965. He received the M.Sc. and Ph.D. degrees in engineering from the Institut National des Sciences Appliquées de Lyon (INSA Lyon), Lyon, France, in 1988, 1989, and 1992, respectively.

In 1992, he joined the Centre de Génie Electrique de Lyon, INSA Lyon, University of Lyon, Lyon, as an Assistant Professor; he is currently a Full Professor and the Head Manager of the Ampere Laboratory, Centre National de la Recherche Scientifique, Unité Mixte de Recherche 5005. His research interests include the integration of power systems, either hybrid or monolithic, power semiconductor device modeling and characterization, power-electronic system design, and low-power monolithic converter design. He has led numerous industrial and academic projects. He is the author or coauthor of more than 50 papers and 80 international conference contributions.

Prof. Allard was the European Liaison Member in the IEEE Power Electronics Society AdCom and Member-at-Large. He is an Associate Editor for the Industry Applications Society.

Xavier Jordà was born in Barcelona, Spain, in 1967. He received the B.S. degree from the Universitat Autònoma de Barcelona, Barcelona, in 1990, and the Ph.D. degree from the Institut National des Sciences Apliquées de Lyon, Lyon, France, in 1995.

From 1990 to 1995, he was with the Centre de Génie Eléctrique de Lyon, France, where he was involved in vector control of induction motors, three-phase pulsewidth modulation methods, and ac drives. In 1995, he joined the Power Electronics Group, Instituto de Microbiología Bioquímica–Centre Nacional de Microelectrònica (Spanish National Research Council), Barcelona. His current research interests include thermal management, modeling, and electrothermal characterization of power semiconductor devices and systems. He has authored or coauthored more than 100 research papers published in various journal and conference proceedings.

Pierre Bidan was born in Condom, France, in 1963. He received the M.Sc. degree in electrical engineering and the Ph.D. degree in automatic control systems from the University Paul Sabatier, Toulouse, France, in 1985 and 1989, respectively.

From 1990 to 1997, he was actively engaged in research on industrial system control with the Laboratory of Analysis and Architecture of Systems, French National Scientific Research Center (CNRS). Since 1997, he has been with the Laboratoire des Plasmas et de la Conversion d'Energie (LAPLACE), CNRS Unité Mixte de Recherche 5213, University of Paul Sabatier, where he is currently a Professor in the Department of Electrical Engineering. His current research interests include modeling, identification, and time-domain simulation of electrical systems and associated materials.

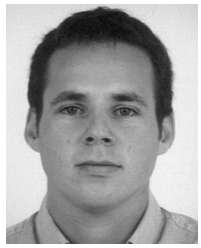

Axel Rumeau was born in Sao Caetano Do Sul, Brazil, in 1980. He received the M.Sc. degree in electronics devices in 2005. He is currently working toward the Ph.D. degree in electrical engineering with the Laboratoire des Plasmas et de la Conversion d'Energie Laboratory, Centre National de la Recherche Scientifique Unité Mixte de Recherche 5213, University of Paul Sabatier, Toulouse, France.

His current research interests include modeling, identification, and time-domain simulation of electrical systems and associated materials.

Hervé Morel (S'07–M'00–SM'07) was born in Reims, France, in 1959. He received the Engineer and Ph.D. degrees from the Ecole Centrale de Lyon, Lyon, France, in 1982 and 1984, respectively.

In 1985, he joined the Centre National de la Recherche Scientifique (CNRS) as an Associated Scientist. He is currently a Senior Scientist with the Ampere Laboratory, Institut National des Sciences Appliquées Lyon, CNRS Unité Mixte de Recherche 5005, University of Lyon, Lyon. His research interests include power semiconductor device characterization and modeling, computer-aided engineering of power electronic system integration, and multiphysic modeling based on bond graphs. He is particularly involves in the design of high-temperature power electronics for the More Electric Aircraft. He is the Manager of SEEDS, the French academic networks on electrical engineering.

Xavier Perpiñà was born in Almenar, Spain, in 1976. He received the B.S. degree in physics in 1999, the M.Phil. degree in electronic engineering in 2002, and the Ph.D. degree in 2005, all from the Universitat Autònoma de Barcelona, Barcelona, Spain.

During 1999, he was involved with the clean room of the Instituto de Microbiología Bioquímica–Centre Nacional de Microelectrònica, Spanish National Research Council (IMB-CNM-CSIC), Barcelona, and then, until 2005, conducted his research activity with the Power Electronics and Systems Group of IMB-CNM-CSIC, where he is currently a Contracted Researcher. From 2005 to 2007, he was with Alstom Transportation, where he was engaged in developing studies on thermal management and power converters reliability. His research interests include the thermal characterization and modeling of power devices using optical methods, as well as the temperature impact on their reliability. He is also involved in studies devoted to analyze the thermal interaction between large insulated gate bipolar transistor modules and their cooling system, and the device failure in the application field. He has authored or coauthored more than 30 research papers published in various conference proceedings and journals.

Miquel Vellvehi was born in Mataró, Spain, in 1968. He received the B.S. degree in physics and the Ph.D. degree in electrical engineering from the Universitat Autònoma de Barcelona, Barcelona, Spain, in 1992 and 1997, respectively.

In 1993, he joined the Power Electronics Group, Instituto de Microbiología Bioquímica–Centre Nacional de Microelectrònica, Spanish National Research Council, Barcelona, where he gained a permanent position in 2007. From 1993 to 1998, his research activities include technology, modeling, and numerical simulation of MOS-controlled power semiconductor devices. Since 1999, his main research activity deals with electrothermal characterization and modeling of power semiconductor devices and circuits. He has authored or coauthored more than 100 research papers published in various journals and conference proceedings.

Sabrine M'Rad, photograph and biography not available at the time of publication.